

# Field experiment of blast wave pressure modulation past a turbulent flow

Takahiro Tamba<sup>\*†</sup>, Daiki Furukawa<sup>\*</sup>, Yuma Aoki<sup>\*</sup>, Masaya Kayumi<sup>\*</sup>, Akira Iwakawa<sup>\*</sup>, Akihiro Sasoh<sup>\*</sup>, Takehiro Matsunaga<sup>\*\*</sup>, Mitsuo Izumo<sup>\*\*</sup>, Yuta Sugiyama<sup>\*\*</sup>, Tomoharu Matsumura<sup>\*\*</sup>, and Yoshio Nakayama<sup>\*\*</sup>

<sup>\*</sup>Department of Aerospace Engineering, Nagoya University,  
Furo-cho, Chikusa-ku, Nagoya, 464-8603, JAPAN  
Phone : +81-52-789-4401

<sup>†</sup>Corresponding author : tamba@fuji.nuae.nagoya-u.ac.jp

<sup>\*\*</sup>National Institute of Advanced Industrial Science and Technology  
1-1-1 Higashi, Tsukuba, Ibaraki, 305-8565, JAPAN

Received : February 4, 2016 Accepted : April 28, 2016

## Abstract

An experimental investigation of the interaction between a quasi-planar blast wave generated by 0.5g report composition and a counter-turbulent flow was conducted in a square field having an area of  $20 \times 15 \text{ m}^2$ . In the experiments, overpressure waveforms of the blast waves were measured using four microphones for both the cases without flow and with turbulence when the speed of natural wind was  $0.0 \text{ m s}^{-1}$ . Without flow, the waveforms were similar to the Friedlander waveform, and the standard deviation between local standardized peak overpressures was 2% of the average of the standardized overpressure. In contrast, with turbulence, the waveforms were modulated between shots, and the standard deviation was 11% of the average of the standardized overpressure.

**Keywords** : field experiment, blast wave, shock wave, turbulence, interaction

## 1. Introduction

Blast wave is a type of shock wave generated by explosions due to rapid expansion of gas and affects buildings at points located far away from the explosion. Even in cases where peak overpressure is less than 1 kPa, a blast wave may damage structures such as window glasses. Therefore, characterization of blast wave impact is important for explosion risk assessment. In addition, it is known that shock waves originating from an airplane flying at supersonic speed cause psychological and physical damages to people, animals, and structures on the ground. This phenomenon is recognized as sonic boom. Previous studies on the evaluation of sonic boom reported that the peak overpressure, the rise time, and the pressure waveform of shock waves were affected by atmospheric turbulence during its propagation<sup>1-3</sup>. In recent years, some studies using direct numerical simulation reported that “wrinkled” or “broken” wave fronts were formed when a weak shock wave interacted with relatively strong

turbulence<sup>4,5</sup>. If a blast wave propagates through a long distance, these modulations of the blast wave may be due to the interaction with turbulence. Therefore, the shock wave-turbulence interaction is an important phenomenon related to risk assessment of blast wave.

Until now, several studies on the shock wave-turbulence interaction have been conducted using various facilities in laboratories. Keller and Merzkirch<sup>6</sup> conducted an experiment on the interaction between a reflected shock wave and grid turbulence in a shock tube. In this experiment, a grid was installed in the flow behind an incident shock wave in order to disturb the flow. Honkan and Andreopoulos<sup>7</sup> and Agui et al.<sup>8</sup> introduced a porous wall as the end wall of a shock tube to control the strength of a reflected shock wave in interaction experiments. These studies reported the effects of the interaction on the integral scale and the root-mean-square (rms) velocity fluctuation of the turbulence.

Bass et al.<sup>9</sup> used supersonic free flight models as shock

wave sources and investigated the interaction of shock waves with atmospheric turbulence. However, an obvious correlation was not observed between the rise time of the shock wave and the strength of the turbulence. Xanthos *et al.*<sup>10)</sup> investigated the interaction between a normal shock wave and grid turbulence by using a shock tube with a porous wall. The result showed that variation of static pressure behind the shock wave increased because of the interaction with the turbulence. Lipkens and Blackstock<sup>11)</sup> generated a normal shock wave by using discharge at the focal point of a parabola for the interaction with turbulent jet. They reported increments in the rise time and the distribution of peak overpressures of the shock waves because of the interaction. Kim *et al.*<sup>12)</sup> visualized the interaction between a spherical shock wave generated by laser breakdown and turbulent jet. The result showed the correlation between the modulation of peak overpressure and that of the wave front of the shock wave. Ribner *et al.*<sup>13)</sup> and Sasoh *et al.*<sup>14)</sup> used open-end shock tubes as shock wave sources. Ribner *et al.* observed the modulation of the waveform and an increment in the rise time of the shock wave due to the interaction with counter-turbulent jet. Sasoh *et al.* reported that the standard deviation in peak overpressures increased to more than four times when the shock wave interacted with grid turbulence.

Thus, many researchers have reported the modulation of shock wave characteristics through the interaction with turbulence. However, it is not easy to realize the shock wave-turbulence interaction while controlling the strengths of the shock wave and the turbulence independently. Using a shock tube<sup>6)–8), 10)</sup>, a normal shock wave, which is suitable for quantitative evaluations, can be applied to experiments. Tamba *et al.*<sup>15)</sup> developed a “counter-driver shock tube,” in which two drivers on both ends of a shock tube can be operated with independent driver conditions; their operation timings are controlled using electrical signals. Using this device, experiments of the interaction between a normal shock wave and grid turbulence can be done with setting their conditions independently. However, a shock wave generated in shock tube cannot be so weak as of Mach 1.01 or even lower because it is difficult to rupture the cellophane diaphragms with a very small pressure difference. Using a blast-type shock wave to investigate the behavior of a weak shock wave near the explosion point or an equivalent point to that<sup>9), 12)–14)</sup>, the shock wave is rapidly attenuated. In the case of using a reflected shock wave from a parabola<sup>11)</sup>, the region where the shock wave can be regarded as a normal shock wave is quite limited because of the effect of expansion waves propagating from the edge of the parabola.

In contrast, a blast wave generated by explosion is nearly spherical in far field. Although the non-planarity effect cannot be ignored near the explosion point, the radius of curvature of the blast wave becomes larger when the blast wave propagates a sufficient distance in the field. If it is applied to the study of the turbulence interaction, the blast wave can be regarded as a quasi-normal shock wave in the interaction region. In this

method, the sufficient state can be realized to investigate the characteristics of the rising of the shock wave. However, a large experimental system is necessary, as the blast wave has to propagate a sufficient distance from the explosion point. Therefore, in this study, an interaction experiment between a quasi-normal blast wave, which propagated a distance of several meters, and a counter-turbulent flow was conducted in a field. The purpose of this study is to construct a model of an experimental system for investigating the interaction between blast wave and turbulence and to demonstrate its effectiveness.

## 2. Experimental

### 2.1 Apparatus

Figure 1 shows the experimental setup, and Figure 2 shows the image of the experimental field. The experiments were conducted in a field located in the premises of the National Institute of Advanced Science and Technology in Tsukuba, Japan. The area of the experimental field was  $20 \times 15 \text{ m}^2$ . Blast wave sources and a turbulence generator were set in the field, and the pressure waveforms of blast waves were measured using microphones. Moreover, a natural wind anemometer (Windworks, Field Pro) was installed at the top of the turbulence generator to measure the speed of natural wind.

Figure 3 shows the image of the blast wave source. A paper tube filled with a report composition (KP : Al : S = 65 : 19 : 16) of 0.5 g was held by a fuse at a height of 1000 mm from the ground and 6000 mm from the grid, as also shown in Figure 1. The report composition was ignited by the combustion of a fuse head using an electric signal, and blast wave was generated.

The turbulence generator was composed of a blower (SF-45MS-1VP, Suiden, fan diameter 450 mm), a duct having a square cross section, and a square grid, as shown in Figure 1. The height of the central axis of the turbulence generator was set to 1000 mm, which was the same as that of the blast wave sources. The flow induced by the blower was contracted and passed through the 600-mm strait duct. Then the flow was blown down through the nozzle having a square cross section of  $340 \times 340 \text{ mm}^2$

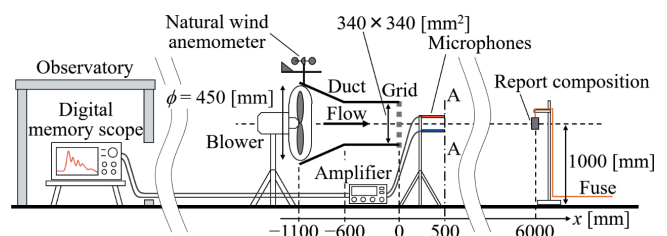


Figure 1 Experimental setup.



Figure 2 Image of experimental field.

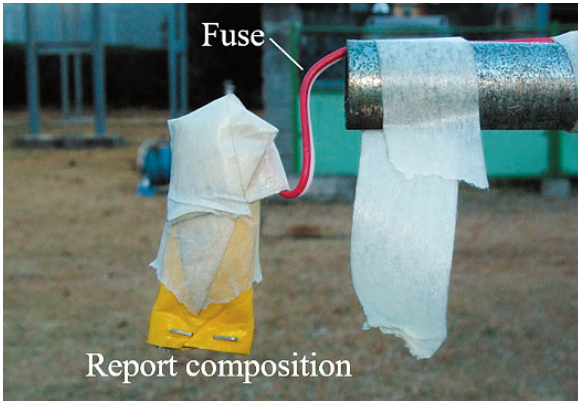


Figure 3 Image of blast wave source.

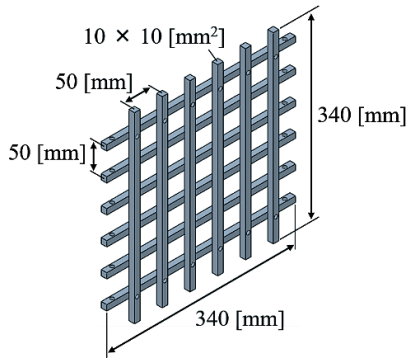


Figure 4 Square grid, solidity = 36%.

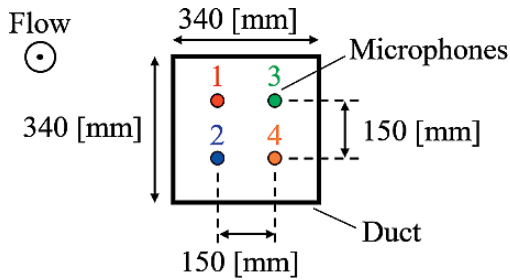


Figure 5 Arrangement of microphones, A-A cross section ( $x = 500\text{ mm}$ ) in Figure 1, 1 to 4 are microphone numbers.

in a direction opposite to that of the blast wave in order to increase the interaction distance. A square grid was set on the nozzle to disturb the flow passing through the grid. Figure 4 shows the schematics of the square grid. The grid was composed of  $10 \times 10\text{ mm}^2$  square pillars, which crossed each other at intervals of 50 mm. The solidity of the grid was 36%.

The pressure waveforms of the blast waves were measured using four microphones (4939-A-011, Brüel & Kjær, frequency range 4 Hz – 100 kHz). Figure 5 shows the arrangement of the microphones. The microphones were symmetrically installed in the path of the turbulent flow induced by the turbulence generator in a direction opposite to that of the blast wave, as also shown in Figure 1. The microphone heads were located at a distance of 500 mm from the grid, and the interval between the microphones was 150 mm. The signals obtained from the microphones were amplified using an amplifier and measured by a digital memory scope in an observatory.

## 2.2 Characteristics of turbulence

The characteristics of the turbulent flow induced by the turbulence generator were obtained from flow velocity measurement using a hot-wire anemometer in an indoor laboratory. Figure 6 shows the distribution of turbulent characteristics in the flow direction. To obtain the characteristics, the hot-wire anemometer was set at the position of microphone 1 (Figure 5) and swept in a parallel direction to the central axis of the turbulence generator.

Figure 6 (a) shows that the time-averaged flow velocity  $U_\infty$  decreased as the distance from the nozzle increased. In contrast, Figure 6 (b) presents that the rms velocity fluctuation  $u'$  was about  $0.8\text{ m s}^{-1}$ . It did not vary greatly in the range of  $500\text{ mm} < x < 2000\text{ mm}$ . When the speed of sound in the atmosphere was  $a_\infty = 340\text{ m/s}$ , the turbulent Mach number was  $M_t = \sqrt{3/2}u'/a_\infty \approx 2.9 \times 10^{-3}$ . The integral length scale  $L_i$ , which represents the average vortex scale in turbulence, was calculated from the rms velocity fluctuation. As shown in Figure 6 (c), although the integral length scale decreased as the distance from the nozzle increased, it was still 58 mm at  $x = 2000\text{ mm}$ .

The turbulent characteristics were also measured in the plane at  $x = 500\text{ mm}$ . Although the time-averaged flow speeds at the position of the four microphones were  $u = 4.0 - 4.8\text{ m/s}$ , whereas the flow speed at the central axis of the nozzle was lower,  $u = 2.9\text{ m/s}$ , due to the blockage on the rotation axis of the fan. It indicates the distribution of the average flow velocity in the same plane. In contrast, the rms velocity fluctuation at the central axis of the nozzle was  $u' = 0.7\text{ m/s}$ . The value was close to those observed at the positions of the four microphones, which ranged between  $0.6 - 0.9\text{ m/s}$ .

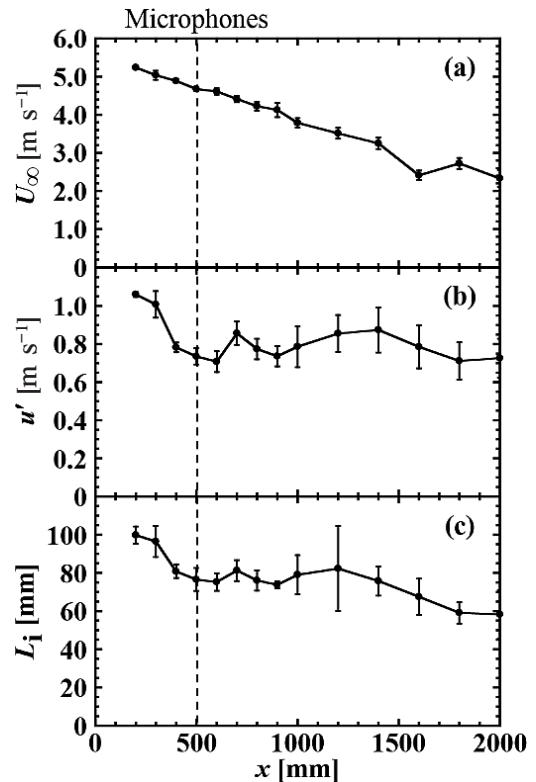


Figure 6 Characteristics of turbulence, (a)  $U_\infty$ , (b)  $u'$ , (c)  $L_i$ , horizontal axis  $x$  is the distance from the nozzle of turbulence generator.

**Table 1** Experimental conditions.

|                             | Weather | Atmospheric pressure [kPa] | Temperature [°C] | Humidity [%] | Natural wind [ $\text{ms}^{-1}$ ] | Shot number (without flow / with turbulence) |
|-----------------------------|---------|----------------------------|------------------|--------------|-----------------------------------|--|
| Day 1<br>(December 3, 2014) | Sunny   | 101.0–101.2                | 11–17            | 26–29        | 0.0                               | 5 / 10                                       |
| Day 2<br>(December 4, 2014) | Cloudy  | 100.7–100.8                | 11–13            | ~68          | 0.0                               | 3 / 7  |

### 2.3 Conditions

The experiments were conducted over two days. The experimental conditions are described in Table 1. To evaluate the effect of the turbulent flow induced by the turbulence generator on the blast waves, the blast wave sources were exploded when the natural wind, speed monitored using the natural wind anemometer, was  $0.0 \text{ m s}^{-1}$ . In the experiments, five shots were performed in Day 1, and three shots were performed in Day 2, for the case where the blast waves propagated without the turbulent flow (referred to as “without flow”). Furthermore, ten shots were performed in Day 1, and seven shots were performed in Day 2, for the case where the blast waves propagated through the turbulent flow induced by the turbulence generator (referred to as “with turbulence”).

### 2.4 Pressure signal correction

A typical fast-response pressure transducer is composed of a thin metal diaphragm and a quartz disk or a capacitor. When a waveform of a shock wave is measured using the pressure transducer, a device function that originates from the mechanical oscillation of the sensor caused by an impact of the shock wave is convoluted to a signal of the pressure waveform. To obtain the original waveform, it is necessary to calibrate and remove the device function, which is artifact. Therefore, the waveforms measured by the microphones were corrected through a deconvolution process<sup>14),16)</sup> by using numerical Laplace transform<sup>17)</sup> to recover the pressure waveforms. The detailed process can be found in Ref. 14.

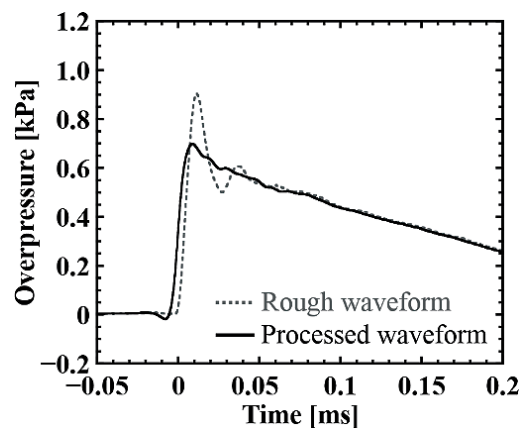
Using a shock tube, the device function of a microphone was obtained from overpressure measurement behind a normal shock wave; the device function could be calculated by using a numerical Laplace transform when the overpressure history of a normal shock wave was assumed to be a Heaviside function. In this study, the microphones were not set in a completely symmetrical orientation because of the nature of the field experiment; this resulted in spatial errors of approximately 10 mm. These errors caused differences in the arrival times of the blast waves at each microphone. Therefore, the time at which the blast wave arrived at each microphone was set to  $t = 0$  initially, such that the origins of the time axis of each waveform were unified. Then, the waveforms that unified the standard of the time axis were deconvoluted in the range  $-0.1 \leq t \leq 1.7 \text{ ms}$ , and fitted by B-spline functions.

## 3. Results and discussion

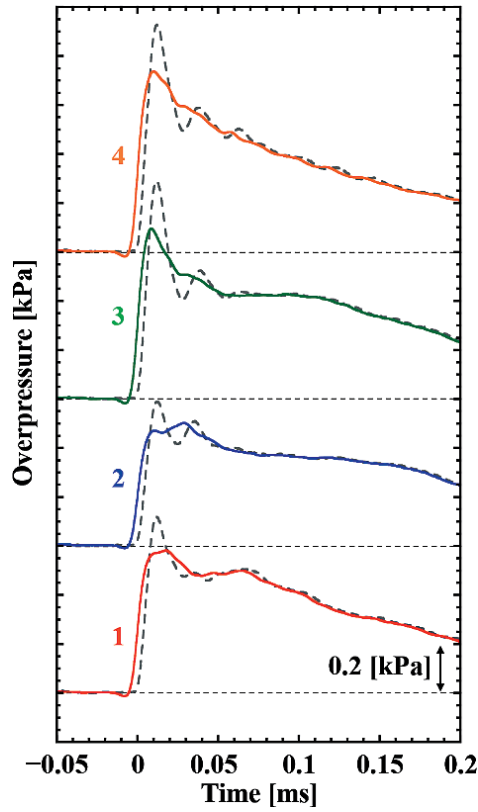
### 3.1 Effect of turbulence on pressure waveform

Figure 7 shows typical examples of a measured waveform in the case without flow (“rough waveform”), and the waveform recovered from the rough waveform by the deconvolution process (“processed waveform”). In the rising of the blast wave, the rough waveform had an overshoot, which was caused because an impact of the blast wave was suddenly applied to the microphone. However, by using the deconvolution process, the processed waveform recovered the original waveform similar to the Friedlander waveform<sup>18)</sup>, which is particular to blast wave. The effective rise time, which is the duration between the time to be 10% of the peak overpressure and the time to be 90% of that, of the processed waveform was  $9 \mu\text{s}$ . The value is consistent to the frequency range of up to 100 kHz. The Mach number of the blast wave calculated from the peak overpressure of the processed waveform was  $M_s = 1.003$ . As the Mach number of the interacted turbulent flow was  $M_t \approx 2.9 \times 10^{-3}$  as shown in section 2.2, the condition of  $M_t > 0.6(M_s - 1)$ , in which “broken” wave front was suggested in numerical studies<sup>4),5)</sup>, was satisfied. In the following sentence, we will discuss the effect of turbulence by using the processed waveforms.

Figure 8 shows typical examples of pressure waveforms in the case with turbulence. The four pressure waveforms were recovered from rough waveforms, which are drawn in dashed lines, measured in the same shot. In comparison to the case without flow (Figure 7, processed waveform), significant modulations of the waveforms occurred just after the rising of the waveforms. Although the effective rise times of waveforms 1 to 4 were 8 to 10  $\mu\text{s}$ , waveform 1



**Figure 7** Typical example of signal correction (without flow), processed waveform is recovered from rough waveform by deconvolution.



**Figure 8** Typical examples of processed pressure waveforms in one shot (with turbulence), dashed lines are rough waveforms, 1 to 4 correspond to microphone numbers in Figure 5.

and 2 took a significant amount of time to attain its peak from the start of rising. In waveform 1 it took  $18 \mu\text{s}$  for the overpressure reached a maximum; in waveform 2,  $29 \mu\text{s}$ . This period was two to three times longer than the effective rise time. In waveform 3 and 4, the periods were  $9 \mu\text{s}$  and  $10 \mu\text{s}$ , respectively, which were comparable to the effective rise time. In addition, the peak overpressures were also affected by turbulence. The peak overpressure of waveform 2 was  $0.502 \text{ kPa}$ , which was relatively lower, and the high pressure behind the blast wave was maintained for a longer duration compared to the other waveforms. In contrast to waveform 2, waveform 4 had a strong peak overpressure, which was  $0.737 \text{ kPa}$ , just after the rising.

### 3.2 Evaluation of reproducibility and error of setup

As this study was conducted in a field, experimental data were affected by uncertainty of the location of a blast wave source. In this section, the influences of associated errors will be evaluated.

Let  $i$  be the serial shot number of shot ( $1 \leq i \leq N$ ),  $j$  be the microphone number ( $1 \leq j \leq K$ ,  $K=4$ ). Also, let  $\Delta P(i, j)$  be the peak overpressure in the  $i$ -th shot and at the microphone  $j$ . In the case without flow, the shots of  $1 \leq i \leq 5$  were performed in Day 1 and those of  $6 \leq i \leq 8$  were performed in Day 2. In addition, in the case with turbulence, the shots of  $1 \leq i \leq 10$  were performed in Day 1 and those of  $11 \leq i \leq 17$  were performed in Day 2 (see Table 2). The average overpressures in the  $i$ -th shot  $\overline{\Delta P(i)}$  is given by Equation (1).

**Table 2** Histories of  $\overline{\Delta P(i)}$ , serial shot number  $i$ .

| (a) without flow |       |                                | (b) with turbulence |       |                                |
|------------------|-------|--------------------------------|---------------------|-------|--------------------------------|
| $i$              | day   | $\overline{\Delta P(i)}$ [kPa] | $i$                 | day   | $\overline{\Delta P(i)}$ [kPa] |
| 1                |       | 0.715                          | 1                   |       | 0.629                          |
| 2                |       | 0.687                          | 2                   |       | 0.769                          |
| 3                | Day 1 | 0.654                          | 3                   |       | 0.726                          |
| 4                |       | 0.676                          | 4                   |       | 0.718                          |
| 5                |       | 0.583                          | 5                   | Day 1 | 0.719                          |
| 6                |       | 0.720                          | 6                   |       | 0.673                          |
| 7                | Day 2 | 0.798                          | 7                   |       | 0.576                          |
| 8                |       | 0.794                          | 8                   |       | 0.698                          |
|                  |       |                                | 9                   |       | 0.618                          |
|                  |       |                                | 10                  |       | 0.591                          |
|                  |       |                                | 11                  |       | 0.806                          |
|                  |       |                                | 12                  |       | 0.897                          |
|                  |       |                                | 13                  |       | 0.889                          |
|                  |       |                                | 14                  | Day 2 | 0.945                          |
|                  |       |                                | 15                  |       | 0.933                          |
|                  |       |                                | 16                  |       | 0.935                          |
|                  |       |                                | 17                  |       | 0.875                          |

**Table 3**  $\overline{\Delta P}$  and  $\sigma_s$  (without flow).

|                             | Day 1 ( $1 \leq i \leq 5$ ) | Day 2 ( $6 \leq i \leq 8$ ) |
|-----------------------------|-----------------------------|-----------------------------|
| $\overline{\Delta P}$ [kPa] | 0.663                       | 0.771                       |
| $\sigma_s$ [kPa]            | 0.045                       | 0.036                       |

**Table 4**  $\overline{\Delta P}$  and  $\sigma_s$  (with turbulence).

|                             | Day 1 ( $1 \leq i \leq 10$ ) | Day 2 ( $11 \leq i \leq 17$ ) |
|-----------------------------|------------------------------|-------------------------------|
| $\overline{\Delta P}$ [kPa] | 0.672                        | 0.897                         |
| $\sigma_s$ [kPa]            | 0.062                        | 0.044                         |

$$\overline{\Delta P(i)} = \frac{1}{K} \sum_{j=1}^K \Delta P(i, j) \quad (1)$$

Let the shots that were conducted in a day be  $m \leq i \leq n$ . The average overpressure in the day  $\overline{\Delta P}$  and the standard deviation caused by the reproducibility  $\sigma_s$  are given by Equations (2) and (3), respectively.

$$\overline{\Delta P} = \frac{1}{n-m+1} \sum_{i=m}^n \overline{\Delta P(i)} \quad (2)$$

$$\sigma_s = \sqrt{\frac{1}{n-m+1} \sum_{i=m}^n \{\overline{\Delta P(i)} - \overline{\Delta P}\}^2} \quad (3)$$

Table 2 shows the histories of  $\overline{\Delta P(i)}$  for each condition. Table 3 shows  $\overline{\Delta P}$  and  $\sigma_s$  in the case without flow, and Table 4 shows those in the case with turbulence. In the case without flow, Table 3 shows that the difference between the values of  $\overline{\Delta P}$  for Day 1 and Day 2 was approximately  $0.1 \text{ kPa}$ . The cause of the difference was that the relative positions of each microphone for the blast wave source had small errors over the two days. Moreover, even for the same day,  $\overline{\Delta P(i)}$  varied for each

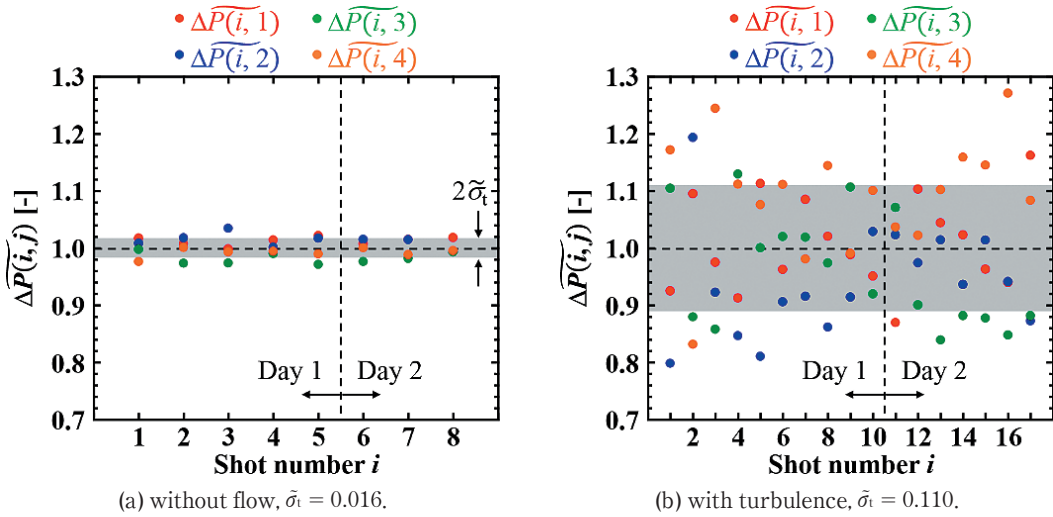


**Figure 9** Distribution of standardized peak overpressure  $\Delta\overline{P}(i, j)$ ,  $j$  corresponds to microphone numbers in Figure 5.

shot, and  $\sigma_s$  was 7% of  $\overline{\Delta P}$  in maximum, as shown in Table 2 and 3, respectively. The primary cause for  $\sigma_s$  was uncertainty in the mass of the report composition, the direction and position of the paper tube in which the report composition was contained. In the case with turbulence, Table 4 shows that  $\overline{\Delta P}$  was larger than that in the case without flow for the same day because the propagation through the counter flow caused an increment in the relative Mach number. Under this condition,  $\sigma_s$  was less than 9% of  $\overline{\Delta P}$  in maximum. Although the ratio of  $\sigma_s$  for  $\overline{\Delta P}$  was 30% larger than that in the case without flow, the result indicated that  $\overline{\Delta P}$  in this case had reproducibility equal to that in the case without flow.

### 3.3 Effect of turbulence on standard deviation of peak overpressure

In this section, the effect of the turbulence on the blast wave will be evaluated. To extract the effect only of the turbulence,  $\Delta P(i, j)$  is standardized by  $\overline{\Delta P}(i)$  in each shot. The standardized peak overpressure  $\Delta\overline{P}(i, j)$  is given by Equation (4).

$$\Delta\overline{P}(i, j) = \frac{\Delta P(i, j)}{\overline{\Delta P}(i)} \quad (4)$$

The average of the entire  $\Delta\overline{P}(i, j)$  is unity. Using Equation (4), the standard deviation caused by the local modulation of the standardized peak overpressures  $\sigma_{\tilde{i}}$  is given by Equation (5).

$$\sigma_{\tilde{i}} = \sqrt{\frac{1}{KN} \sum_{i=1}^N \sum_{j=1}^K \{\Delta\overline{P}(i, j) - 1\}^2} \quad (5)$$

Figure 9 shows the distributions of  $\Delta\overline{P}(i, j)$  in each shot and at each microphone. The gray belts in Figure 9 represent the width of  $2\sigma_{\tilde{i}}$ . In the case without flow (Figure 9 (a)), the standard deviation in  $\Delta\overline{P}(i, j)$  was relatively small,  $\sigma_{\tilde{i}} = 0.016$ , which was 2% of the average of the entire  $\Delta\overline{P}(i, j)$ . One of possible reasons why  $\sigma_{\tilde{i}}$  was not zero is that it was affected by the turbulence induced by the natural wind before performing the shot, and the non-uniform distribution of atmospheric temperature.

However, the result indicated that the blast waves propagated almost uniformly. In contrast, in the case with turbulence, Figure 9 (b) shows that  $\Delta\overline{P}(i, j)$  greatly scattered in each shot and at each microphone. The standard deviation in  $\Delta\overline{P}(i, j)$  was  $\sigma_{\tilde{i}} = 0.110$ , which was 11% of the average of the entire  $\Delta\overline{P}(i, j)$ . This value was quite large compared to the value obtained in the case without flow;  $\sigma_{\tilde{i}}$  in this case was 7 times larger than that without flow;  $\sigma_{\tilde{i}}$  in this case was 7 times larger than that without flow. On the other hand,  $\Delta\overline{P}(i, j)$  obtained at each microphone had non-negligible deviations. For example, most of  $\Delta\overline{P}(i, 2)$  in Day 1 and  $\Delta\overline{P}(i, 3)$  in Day 2 were distributed in the region less than  $\Delta\overline{P}(i, j) = 1.0$ , which is the average of the entire  $\Delta\overline{P}(i, j)$ . In contrast, most of  $\Delta\overline{P}(i, 4)$  in Days 1 and 2 were more than  $\Delta\overline{P}(i, j) = 1.0$ . It can be explained by the following reason; the installation error of the blower in the turbulence generator caused distortion of the average flow, which affected the relative Mach numbers of the blast waves. However,  $\Delta\overline{P}(i, j)$  at each microphone greatly varied for different shots, and the variations in each microphone were obviously larger than those in the case without flow. It indicated that the peak overpressure of the blast waves were modulated through the interaction with turbulent flow.

## 4. Conclusion

In this study, an experimental system for investigating the interaction between a quasi-normal shock wave generated by explosion and a counter-turbulent flow in a field was developed. Using the system, multipoint pressure measurements were conducted; a total of 8 shots were performed for the case without flow, and a total of 17 shots were performed for the case with turbulence.

When the experiments were conducted in the case without flow, pressure waveforms that were similar to the Friedlander waveform were observed. The standard deviation originating from the local modulation of the standardized peak overpressure was 2% of the average of the standardized peak overpressure. It means that the blast waves propagated in almost uniformly. In contrast, in the case with turbulence, the peak overpressure greatly varied for each shot and at each measured point. The

standard deviation originating from the local modulation was 11% of the average of the standardized peak overpressure. In this case, overpressures at each point had some spatial deviations because of the installation error of the turbulence generator. However, the variations in peak overpressures at each point were obviously larger than those in the case without flow.

### Acknowledgement

This study was supported by Japan Society for Promotion of Science (JSPS) "KAKENHI" through a Challenging Exploratory Research No. 26630442.

### References

- 1) H. H. Hubbard, D. J. Maglieri, V. Huckel, and D. A. Hilton, NASA TR R-198 (1964).
- 2) D. J. Maglieri and D. A. Hilton, NASA TN D-3520 (1966).
- 3) I. E. Garrick and D. J. Maglieri, NASA TN D-4588 (1968).
- 4) D. D. Donzis, *Phys. Fluids*, 24, 126101 (2012).
- 5) J. Larsson, I. Bermejo-Moreno, and S. K. Lele, *J. Fluid Mech.*, 717, 293–321 (2013).
- 6) J. Keller and W. Merzkirch, *Exp. Fluids*, 8, 241–248 (1990).
- 7) A. Honkan and J. Andreopoulos, *Phys. Fluids A*, 4, 2562–2572 (1992).
- 8) J. H. Agui, G. Briassulis, and Y. Andreopoulos, *J. Fluid Mech.*, 524, 143–195 (2005).
- 9) H. E. Bass, B. A. Layton, and L. N. Bolen, *J. Acoust. Soc. Am.*, 82, 306–310 (1987).
- 10) S. Xanthos, G. Briassulis, and Y. Andreopoulos, *J. Propul. Power*, 18, 1289–1297 (2002).
- 11) B. Lipkens and D. T. Blackstock, *J. Acoust. Soc. Am.*, 103, 148–158 (1997).
- 12) J. H. Kim, A. Sasoh, and A. Matsuda, *Shock Waves*, 20, 339–345 (2010).
- 13) H. S. Ribner, P. J. Morris, and W. H. Chu, *J. Acoust. Soc. Am.*, 53, 926–928 (1973).
- 14) A. Sasoh, T. Harasaki, T. Kitamura, D. Takagi, S. Ito, A. Matsuda, K. Nagata, and Y. Sakai, *Shock Waves*, 24, 489–500 (2014).
- 15) T. Tamba, T. M. Nguyen, K. Takeya, T. Harasaki, A. Iwakawa, and A. Sasoh, *Shock Waves*, 25, 667–674 (2015).
- 16) H. Inoue, H. Ishida, K. Kishimoto, and T. Shibuya, *JSME International Journal Ser. 1*, 34, 453–458 (1991).
- 17) D. J. Wilcox, *Int. J. Elect. Enging Educ.*, 15, 247–265 (1978).
- 18) F. G. Friedlander, *Proc. R. Soc. Lond. A*, 186, 322–344 (1946).